Colloids and Surfaces B: Biointerfaces 107 (2013) 257–261

Contents lists available at SciVerse ScienceDirect

Colloids and Surfaces B: Biointerfaces

journal homepage: www.elsevier.com/locate/colsurfb

Short communication

Electrochemical impedimetric DNA sensing based on multi-walled carbon nanotubes–SnO_2–chitosan nanocomposite

Tao Yang, Xiuhong Guo, Yao Ma, Qianhe Li, Ling Zhong, Kui Jiao*

Key Laboratory of Eco-chemical Engineering (Ministry of Education), College of Chemistry and Molecular Engineering, Qingdao University of Science and Technology, Qingdao 266042, China

ARTICLE INFO

Article history:
Received 19 June 2012
Received in revised form 11 January 2013
Accepted 17 January 2013
Available online 30 January 2013

Keywords:
Multi-walled carbon nanotubes
SnO_2 nanoparticles
PAT gene
DNA biosensor

ABSTRACT

A sensitive electrochemical impedimetric DNA biosensor based on the integration of tin oxide (SnO_2) nanoparticles, chitosan (CHIT) and multi-walled carbon nanotubes (MWNTs) is presented in this paper. The MWNTs–SnO_2–CHIT composite modified gold electrode was characterized by cyclic voltammetry (CV) and electrochemical impedance spectroscopy (EIS). Compared with individual MWNTs–CHIT, SnO_2–CHIT and bare gold electrode, this composite showed the most obvious electrochemical signal of the redox probe $[Fe(CN)_6]^{3-/4-}$. According to the change of the electron transfer resistance (R_{et}) induced by the hybridization, target DNA was successfully detected via EIS. This DNA electrochemical biosensor was applied to detect phosphinothricin acetyltransferase (PAT) gene in transgenic corn. The synergistic effect of the MWNTs–SnO_2–CHIT remarkably enhanced DNA immobilization and hybridization detection. The dynamic detection range was from 1.0×10^{-11} mol/L to 1.0×10^{-6} mol/L with a detection limit of 2.5×10^{-12} mol/L. This sensing platform showed inner advantage, such as simplicity, good stability, and high sensitivity.

1. Introduction

Recently, the porous, low-temperature sol–gel-obtained inorganic oxide nanomaterials have attracted widespread interest as ideal materials for biomolecule immobilization due to their tunable porosity, high thermal and chemical stability. The nanostructures of these inorganic oxide could greatly enhance the active surface area, as well as promote the electron transfer process between the biomolecules and the electrodes [1,2]. Among these inorganic oxide films, tin oxide (SnO_2), a stable large band-gap (330 nm) metal oxide semiconductor with an isoelectricpoint (IEP about 5), has been extensively used in the microelectronics, photoelectronics, solar cells, and biosensing devices since its excellent photoelectronic property, high sensitivity and a short response time, meanwhile relatively higher conductivity than TiO_2 and SiO_2 [3–6]. However, as a kind of inorganic semiconductor oxide with a large specific surface area, no toxicity and high activity, SnO_2 and its composites have been scarcely used in DNA electrochemical sensors [7]. At the same time, as a star nanomaterial, carbon nanotubes have been widely used in DNA electrochemical sensors [8–11] due to its high surface area, excellent electron transport capacity, high chemical stability, and outstanding catalytic ability [12–15]. Meanwhile, as an attractive biocompatible, biodegradable and nontoxic natural biopolymer, chitosan (CHIT) is widely adopted in the nanocomposites fabrication for electrochemical DNA detection due to its excellent film-forming ability [16–18].

In this research, the nanocomposite of multi-walled carbon nanotubes (MWNTs), SnO_2 and CHIT, which grafted the advantages of individual participation to reveal synergistic effect, was fabricated to construct electrochemical DNA hybridization sensor. The experimental results showed that MWNTs–SnO_2–CHIT nanocomposite modified gold electrode could obviously prompt the electrochemical response of $[Fe(CN)_6]^{3-/4-}$ compared with MWNTs–CHIT/Au and SnO_2–CHIT/Au. To our best knowledge, MWNTs–SnO_2–CHIT nanocomposite, which possesses highly electrode surface active area, plenty of electrochemical sites, and super conductivity, has not been reported for electrochemical DNA detection.

2. Experimental

2.1. Apparatus and reagents

Apparatus: The electrochemical experiments were performed with a CHI660C electrochemical analyzer (Shanghai CH Instrument Company, China), with Au or modified Au working electrode, a platinum wire auxiliary electrode, and a saturated calomel reference electrode (SCE). Scanning electron microscopy (SEM) was carried

* Corresponding author Tel.: +86 053284022858.
E-mail addresses: kjiao@qust.edu.cn, taoyang@qust.edu.cn (K. Jiao).

0927-7765/$ – see front matter.
http://dx.doi.org/10.1016/j.colsurfb.2013.01.046

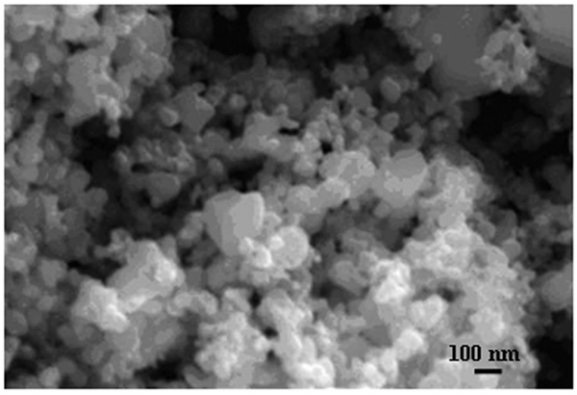

Fig. 1. The SEM image of SnO_2 nanoparticles.

out using a JSM-6700F machine (JEOL, Tokyo, Japan). The pH values of all solutions were measured by a model pHS-25 digital acidimeter (Shanghai Leici Factory, China). All solutions were prepared with Aquapro ultrapure water (Ever Young Enterprises Development. Co., Ltd., Chongqing, China).

Materials: The nano-SnO_2 was prepared by the sol–gel method [19] and related SEM image was shown in Fig. 1. MWNTs (purity > 95%) was purchased from Shenzhen Nanotech Port Company (China) and CHIT was purchased from Shanghai Chemical Reagent Company (China).

The 20-base oligonucleotides probe (ssDNA), its complementary DNA sequence (cDNA, target DNA, namely a 20-base fragment of phosphinothricin acetyltransferase (PAT) gene sequence, which was selected according to PAT transgenic sequence) were synthesized by Beijing SBS Gene Technology Limited Company. The stock solutions were same as Ref. [8]. Their base sequences are listed below:

probe DNA (ssDNA): 5′-GCC ACA AAC ACC ACA AGA GT-3′
target DNA: 5′-ACT CTT GTG GTG TTT GTG GC-3′

2.2. Preparation of MWNTs–SnO_2–CHIT/Au

The Au electrode surface was freshly polished with 0.3 μm and 0.05 μm alumina powder, respectively, and then rinsed with ultrapure water after each polishing, finally cleaned ultrasonically with 95% ethanol and acetone for 3 min, respectively.

The SnO_2 nanoparticles and MWNTs with a mass ratio of 1:3 were dispersed in 0.2% CHIT solution and stirred at room temperature for 3 h. The obtained highly dispersed black suspension would be named as MWNTs–SnO_2–CHIT. A 10 μl of MWNTs–SnO_2–CHIT suspension was coated on the Au electrode surface and air-dried naturally to obtain MWNTs–SnO_2–CHIT/Au.

Similarly, SnO_2–CHIT/Au and MWNTs–CHIT/Au were prepared under the same procedure as illustrated in MWNTs–SnO_2–CHIT/Au preparation just without MWNTs or SnO_2 existing, respectively.

2.3. Immobilization and hybridization of DNA

The immobilization of probe DNA on the MWNTs–SnO_2–CHIT/Au electrode was incubated at room temperature in a Tris–HCl buffer solution containing 1.0×10^{-6} mol/L ssDNA probe for 1 h, followed by washing the electrode with 0.2% sodium dodecylsulfate solution (SDS, 0.2% $CH_3(CH_2)_{10}CH_2SO_3Na$) and ultrapure water to remove the unbound ssDNA probe for 5 min, respectively. The obtained electrode was noted as ssDNA/MWNTs–SnO_2–CHIT/Au.

The ssDNA/MWNTs–SnO_2–CHIT/Au was placed in a hybridization solution containing different concentrations of target DNA at 45 °C for 45 min. Then the obtained electrodes (dsDNA/MWNTs–SnO_2–CHIT/Au) were washed with 0.2% SDS solution and ultrapure water for 5 min, respectively, to remove the unbound target DNA.

2.4. Electrochemical measurements

Cyclic voltammetry (CV) was carried out in 1.0 mmol/L $[Fe(CN)_6]^{3-/4-}$ (1:1) solution containing 0.1 mol/L KCl with a scan rate of 50 mV/s. Electrochemical impedance spectroscopy (EIS) measurement was performed in the same supporting electrolyte above, with the AC voltage amplitude 5 mV, the voltage frequencies from 10^4 Hz to 0.1 Hz and the applied potential 0.172 V vs. SCE.

The reported result for every electrode in this paper was the mean value of three parallel measurements.

3. Results and discussion

3.1. Electrochemical characterization of MWNTs–SnO_2–CHIT

To investigate the role of the individual component and the possible synergistic effects between MWNTs–SnO_2–CHIT, the CV responses of $[Fe(CN)_6]^{3-/4-}$ at the bare Au electrode and different modified electrodes were studied, respectively, as shown in Fig. 2A. It can be seen that a pair of obvious redox peaks with i_{pc} of 1.13×10^{-5} A and i_{pa} of 1.11×10^{-5} A appears at the bare Au electrode (curve a). The peak currents of the MWNTs–CHIT/Au (curve c, i_{pc} 1.31×10^{-5} A and i_{pa} 1.30×10^{-5} A) increase since the large specific surface area and good conductivity of MWNTs. However, the lowest peak currents with i_{pc} of 8.85×10^{-6} A and i_{pa} of 6.64×10^{-6} A were obtained at the SnO_2–CHIT/Au (curve d) due to the poor electrical conductivity of the SnO_2. The highest redox peaks (i_{pc},1.80×10^{-5} A and i_{pa}, 1.40×10^{-5} A) at the MWNTs–SnO_2–CHIT/Au (curve b) indicate that the synchronous introduction of MWNTs, SnO_2 and CHIT would amplify the peak currents of $[Fe(CN)_6]^{3-/4-}$ compared with bare Au electrode, MWNTs–CHIT/Au, and SnO_2–CHIT/Au. This could be ascribed to the effective integration of individual advantages of MWNTs, SnO_2, and CHIT (such as large surface area, good catalytic activity, and excellent electronic conductivity), which revealed synergistic effect for electrochemical response of $[Fe(CN)_6]^{3-/4-}$.

EIS is a powerful tool to monitor the impedance value of the electrode surface during the process of the frequency variation, which is able to offer various properties of the interface of the electrode and the solution, including the electrode impedance, capacity of the electric double-layer and surface electron transfer resistance (R_{et}) [20–22], which can be directly measured as the semicircle diameter of the Nyquist plots. Therefore, the related R_{et} values of above referred electrodes are investigated and shown in Fig. 2B. The high frequency section of the bare Au electrode (curve a) showed an arc with R_{et} (600 Ω), being smaller than R_{et} of the SnO_2–CHIT/Au (curve d, 650 Ω) since the poor electrical conductivity of the SnO_2. As compared with curves a and d, the R_{et} value of curve c (MWNTs–CHIT/Au) declined (R_{et}, 450 Ω) due to the good electronic conductivity and large surface area of MWNTs. The lowest R_{et} of MWNTs–SnO_2–CHIT/Au (curve b, 100 Ω) demonstrated that the MWNTs–SnO_2–CHIT composite could synergistically promote the electrochemical response of $[Fe(CN)_6]^{3-/4-}$ and reduce the R_{et}. The result is also consistent with CV responses in Fig. 2A.

3.2. Optimization of preparation of MWNTs–SnO_2–CHIT

CHIT is an abundant natural biopolymer with excellent film forming ability, which plays an important role in electrochemical

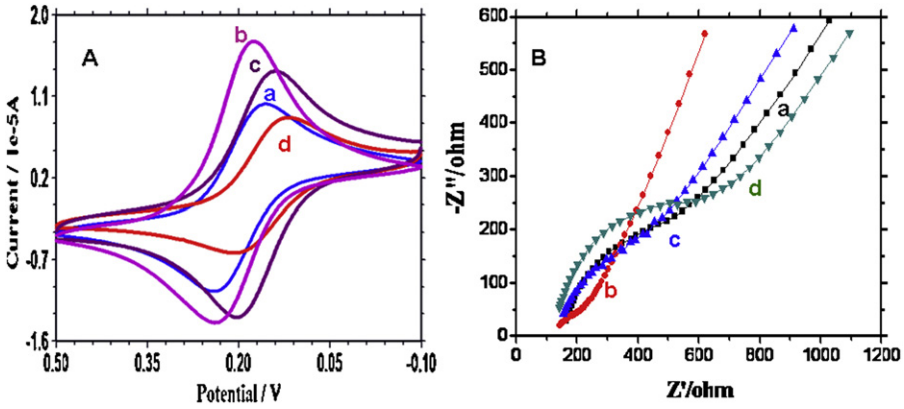

Fig. 2. CVs (A) and representative Nyquist plots (B) recorded at (a) bare Au, (b) MWNTs–SnO_2–CHIT/Au, (c) MWNTs–CHIT/Au and (d) SnO_2–CHIT/Au. Supporting electrolyte solution is 1.0 mmol/L $[Fe(CN)_6]^{3-/4-}$ containing 0.1 mol/L KCl.

sensing platform. So, the selection of CHIT concentration was investigated via CV. The different modified electrodes were prepared by varying CHIT concentration, such as 0.05%, 0.1%, 0.2%, 0.3%, and 0.4%, respectively. CV currents of $[Fe(CN)_6]^{3-/4-}$ at each above electrode were recorded. The current values gradually increased with the increase of the CHIT concentration from 0.05% to 0.2%. Then the current values decreased with further increase of the CHIT concentration. The optimal CHIT concentration was selected as 0.2%.

The same method was adopted to study the effect of stirring time referred in Section 2.2. (preparation of MWNTs–SnO_2–CHIT/Au). The current value rose gradually with the prolongation of the stirring time and then attained a plateau value when the accumulation time reached 3 h or above. Therefore, the stirring time of 3 h was selected in our experiments.

3.3. Immobilization and hybridization of DNA

CVs of $[Fe(CN)_6]^{3-/4-}$ recorded at the MWNTs–SnO_2–CHIT/Au (curve a), ssDNA/MWNTs–SnO_2–CHIT/Au (curve b), dsDNA/MWNTs–SnO_2–CHIT/Au (curve c) are shown in Fig. 3A, where the redox current of $[Fe(CN)_6]^{3-/4-}$ declined in turn. For curve b, after immobilization of DNA, the peak currents decreased dramatically ($i_{pc} = 1.28 \times 10^{-5}$ A, $i_{pa} = 1.11 \times 10^{-5}$ A) as compared with those at the MWNTs–SnO_2–CHIT/Au (curve a, $i_{pc} = 1.80 \times 10^{-5}$ A, $i_{pa} = 1.40 \times 10^{-5}$ A), which could be attributed to the electrostatic repulsion between the anionic redox couple $[Fe(CN)_6]^{3-/4-}$ and the negatively charged phosphate skeletons of DNA immobilized on the MWNTs–SnO_2–CHIT. The successful hybridization of DNA probe with target gene brought more negatively charged DNA phosphate backbone (curve c, $i_{pc} = 0.88 \times 10^{-5}$ A, $i_{pa} = 0.66 \times 10^{-5}$ A), which induced the further decrease of redox currents of $[Fe(CN)_6]^{3-/4-}$ [23,24].

As an effective electrochemical assay method, EIS has been widely adopted for DNA hybridization detection [8,20–22]. The representative Nyquist diagrams for monitoring the immobilization of DNA and hybridization with cDNA sequence are shown in Fig. 3B. The R_{et} of the ssDNA/MWNTs–SnO_2–CHIT/Au (curve b) was higher (1.5×10^3 Ω) than that of the MWNTs–SnO_2–CHIT/Au electrode (curve a, 100 Ω). The increasing of R_{et} could be ascribed to the immobilization of ssDNA. The electronegative phosphate skeletons of DNA prevented the electron transfer during the process of redox reaction ($[Fe(CN)_6]^{3-/4-}$) on the electrode. The further increase of R_{et} (curve c, 2.4×10^3 Ω) showed the successful hybridization of the probe DNA, which brought more electronegative charge [8]. The results were consisted with the results of CVs.

The electrostatic adsorption time of the ssDNA probe had obvious effect on DNA immobilization amount at MWNTs–SnO_2–CHIT/Au electrode. When the electrode was soaked for 1 h or more, the peak current of $[Fe(CN)_6]^{3-/4-}$ on ssDNA/MWNTs–SnO_2–CHIT/Au kept stable. So, 1 h was selected.

The effect of the mass ratio of nano-SnO_2 to MWNTs, such as 1:1, 1:2, 1:3, 1:4, and 1:5, was examined. A small quantity of nano-SnO_2 brought low immobilization amount of ssDNA (less decrease of the peak current of $[Fe(CN)_6]^{3-/4-}$ as compared with those at the MWNTs–SnO_2–CHIT/Au, like that mechanism illustrated in Fig. 3A). While overflowing mass of SnO_2 could contaminate the conductivity of the composite film. Thus 1:3 was chosen.

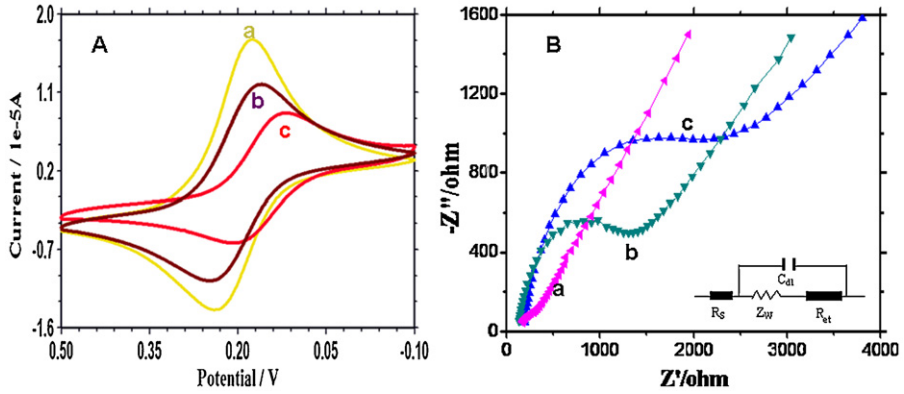

Fig. 3. CVs (A) and representative Nyquist plots (B) recorded at (a) MWNTs–SnO_2–CHIT/Au, (b) ssDNA/MWNTs–SnO_2–CHIT/Au and the probe electrode hybridized with cDNA (c). Supporting electrolyte solution is same to Fig. 2. The inset is model electrical equivalent circuit to describe the data shown in panel B. (1) Electrolyte resistance, R_s; (2) the lipid bilayer capacitance, C_{dl}; (3) charge transfer resistance, R_{et}; (4) Warburg impedance, Z_w.

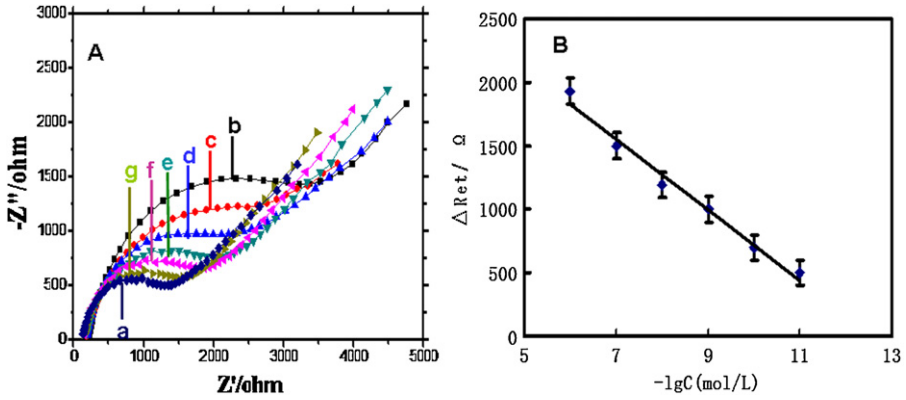

Fig. 4. Nyquist diagrams (A) at ssDNA/MWNTs–SnO_2–CHIT/Au before and after hybridization with the PAT gene fragment of different concentrations (a) ssDNA/MWNTs–SnO_2–CHIT/Au; (b) 1.0×10^{-6}; (c) 1.0×10^{-7}; (d) 1.0×10^{-8}; (e) 1.0×10^{-9}; (f) 1.0×10^{-10}; (g) 1.0×10^{-11} mol/L. The plot of ΔR_{et} vs. the negative logarithm of the PAT gene sequence concentration (B). ΔR_{et} was the difference of impedance values between dsDNA/MWNTs–SnO_2–CHIT/Au electrode and ssDNA/MWNTs–SnO_2–CHIT/Au. Each point is the mean of three measurements, and the error bars correspond to the standard deviation.

To investigate the hybridization temperature and time, the difference of impedance value (ΔR_{et}) between dsDNA/MWNTs–SnO_2–CHIT/Au electrode and ssDNA/MWNTs–SnO_2–CHIT/Au was adopted as signal. The experiments were conducted by placing ssDNA/MWNTs–SnO_2–CHIT/Au electrode in cDNA solution for 10, 20, 30, 40, 50, 60 min, respectively, and then recording the Nyquist diagrams, respectively. The result showed that the largest ΔR_{et} value occurred at 40 min hybridization time. Similarly, the experiments were carried out at different hybridization temperatures such as 25 °C, 35 °C, 45 °C, 50 °C and 55 °C, respectively, for 40 min. The result showed that the ΔR_{et} value increased gradually from 25 °C to 45 °C, and then reached the maximum. Therefore, the hybridization temperature and time were chosen as 45 °C for 40 min, respectively.

3.4. The stability of MWNTs–SnO_2–CHIT membrane and the probe modified electrodes

The stability of the electrochemical DNA sensor is particularly important. MWNTs–SnO_2–CHIT/Au electrodes were placed in 0.1 mol/L NaOH and 0.1 mol/L HCl solutions at room temperature for 3 h, respectively, and no black suspension was observed, which indicated that the MWNTs and nano-SnO_2 were fixed in the CHIT membrane firmly. However, when the composite modified electrodes were soaked in 0.1 mol/L acetic acid solution at room temperature for 1 h, black suspended solids occurred in the solution, which should be ascribed that CHIT is soluble in acetic acid solution inducing the loss of MWNTs and nano-SnO_2 from the surface of modified electrodes.

Furthermore, the ssDNA/MWNTs–SnO_2–CHIT/Au electrodes were placed in ultrapure water, pH 7.0 phosphate buffer, pH 7.0 Tris–HCl buffer, and 2× sodium saline citrate (SSC) buffer solutions for 5 h, respectively. Then the soaked electrodes were measured in 1.0 mmol/L $[Fe(CN)_6]^{3-/4-}$ solution and the CV signal varied little. And further UV–vis experiments (monitoring the soaking solution after ssDNA/MWNTs–SnO_2–CHIT/Au electrode being dipped) showed that no characteristic UV absorption peak occurred at 260 nm for DNA. The results illustrated that the ssDNA/MWNTs–SnO_2–CHIT/Au electrodes kept strong stability.

3.5. The EIS detection for PAT gene fragment

The Nyquist plots of ssDNA/MWNTs–SnO_2–CHIT/Au electrodes hybridized with different concentrations of the PAT gene target sequences from 1.0×10^{-11} mol/L to 1.0×10^{-6} mol/L are shown in Fig. 4A. The ΔR_{et} value between the probe-captured electrode and the hybridized electrode with the cDNA was adopted as measurement signal. The ΔR_{et} value was linear with the negative logarithm of the cDNA concentration in the range of 1.0×10^{-11} mol/L to 1.0×10^{-6} mol/L with a regression equation of ΔR_{et} (Ω) = 278.3 log C + 3502.1 (shown in Fig. 4B, each point was the mean value of three measurements, and the error bars correspond to the standard deviation.). The detection limit was 2.5×10^{-12} mol/L using 3σ, where σ was the standard deviation of 11 parallel measurements of the blank solution.

3.6. Reproducibility and regeneration of the DNA biosensor

A parallel measurement method was applied to investigate the reproducibility of this impedance-based DNA hybridization sensor by adopting a low concentration of target DNA sequence as a model. Five parallel-made DNA sensors were used to detect 1.0×10^{-10} mol/L target DNA sequence and the relative standard deviation (RSD) was 3.7%. The results indicated that the reproducibility of this DNA biosensor was satisfactory.

The regeneration ability of this sensor was also measured by performing repetitive hybridizations according to the specified procedure as illustrated in Ref. [25]. Our constructed sensor could be regenerated for five times without losing its sensitivity, indicating the fine regeneration ability of this biosensor.

4. Conclusion

In summary, a novel MWNTs–SnO_2–CHIT composite film was used as an efficient DNA immobilization platform to fabricate a highly sensitive EIS DNA biosensor. Compared with individual MWNTs–CHIT or SnO_2–CHIT modified electrodes, the experimental results showed that synergistic effect of the MWNTs–SnO_2–CHIT composite film could effectively increase electrochemical signal of $[Fe(CN)_6]^{3-/4-}$, which served as a classic and powerful indicator for label-free DNA EIS detection. The biosensor, which owned highly surface active area, plenty of electrochemical sites, and super conductivity, revealed high sensitivity, low detection limit, and fine stability for the detection of PAT gene fragment.

Acknowledgments

This work was supported by the National Natural Science Foundation of China (Nos. 21275084, 20975057, 20805025), Doctoral Foundation of the Ministry of Education of China (No. 20113719130001), Outstanding Adult-Young Scientific Research Encouraging Foundation of Shandong Province (No. BS2012CL013),

and Scientific and Technical Development Project of Qingdao (No. 12-1-4-3-(23)-jch).

References

[1] P.R. Solanki, M.K. Patel, A. Kaushik, M.K. Pandey, R.K. Kotnala, B.D. Malhotra, Electroanalysis 23 (2011) 2699.
[2] X.Y. Zhang, X.Y. Wang, Y.S. Bai, X.Y. Wang, J.C. Su, J. Electrochem. Soc. 159 (2012) 431.
[3] E. Topoglidis, Y. Astuti, F. Duriaux, M. Gratzel, J.R. Durrant, Langmuir 19 (2003) 6894.
[4] N.Q. Jia, Q. Zhou, L. Liu, M.M. Yan, Z.Y. Jiang, J. Electroanal. Chem. 580 (2005) 213.
[5] A.A. Ansari, A. Kaushik, P.R. Solanki, B.D. Malhotra, Electroanalysis 21 (2009) 965.
[6] M. Muti, A. Erderm, A. Caliskan, A. Sinag, T. Yumak, Colloids Surface B 86 (2011) 154.
[7] M. Muti, F. Kuralay, A. Erdem, S. Abaci, T. Yumak, A. Sinağ, Talanta 82 (2010) 1680.
[8] T. Yang, N. Zhou, Y.C. Zhang, W. Zhang, K. Jiao, G.C. Li, Biosens. Bioelectron. 24 (2009) 2165.
[9] A. Erdem, P. Papakonstantinou, H. Murphy, M. McMullan, H. Karadeniz, S. Sharma, Electroanalysis 22 (2012) 611.
[10] A. Erdem, P. Papakonstantinou, H. Murphy, Anal. Chem. 78 (2006) 6656.
[11] Q.D. Zhang, B. Piro, V. Noël, S. Reisberg, M.C. Pham, Analyst 136 (2011) 1023.
[12] A. Erdem, H. Karadeniz, P.E. Canavar, G. Congur, Electroanalysis 24 (2012) 502.
[13] W. Zhang, T. Yang, X.M. Zhuang, Z.Y. Guo, K. Jiao, Biosens. Bioelectron. 24 (2009) 2417.
[14] J. Wang, G.D. Liu, M.R. Jan, J. Am. Chem. Soc. 126 (2004) 3010.
[15] M.L. Pedano, G.A. Rivas, Electrochem. Commun. 6 (2004) 10.
[16] A. Erdem, M. Muti, H. Karadeniz, G. Congur, E. Canavar, Colloids Surface B 95 (2012) 222.
[17] W. Zhang, T. Yang, D.M. Huang, K. Jiao, G.C. Li, J. Membr. Sci. 325 (2008) 245.
[18] T. Yang, D.M. Huang, Q.H. Li, W. Zhang, K. Jiao, Electroanalysis 24 (2012) 392.
[19] A.S. Ahmed, A. Azam, M.M. Shafeeq, M. Chaman, S. Tabassum, J. Phys. Chem. Solids 73 (2012) 943.
[20] F. Lisdat, D. Schaefer, Anal. Bioanal. Chem. 391 (2008) 1555.
[21] Y.W. Hu, T. Yang, X.X. Wang, K. Jiao, Chem. Eur. J. 16 (2010) 1992.
[22] T. Yang, N. Zhou, Q.H. Li, W. Zhang, K. Jiao, Colloids Surface B 97 (2012) 150.
[23] N.J. Yang, H. Uetsuka, E. Osawa, C.E. Nebel, Angew. Chem. Int. Ed. 47 (2008) 5183.
[24] X.X. Wang, T. Yang, X. Li, K. Jiao, Biosens. Bioelectron. 26 (2011) 2953.
[25] T. Yang, Y.Y. Feng, W. Zhang, S.Y. Ma, K. Jiao, J. Electroanal. Chem. 656 (2011) 140.